



Article

# Dynamic Gelation of Conductive Polymer Nanocomposites Consisting of Poly(3-hexylthiophene) and ZnO Nanowires

Francesca A. Santos, Dana J. Christensen II, Ryan Y. Cox, Spencer A. Schultz, Raymond H. Fernando and Shanju Zhang \*

Department of Chemistry and Biochemistry, California Polytechnic State University, San Luis Obispo, CA 93407, USA; franceska.a.santos@gmail.com (F.A.S.); djc@alexanderti.com (D.J.C.II); ryanc@cardinalpaint.com (R.Y.C.); spencer.schultz@hancockcollege.edu (S.A.S.); rhfernan@calpoly.edu (R.H.F.)

\* Correspondence: szhang05@calpoly.edu

**Abstract:** The sol–gel transition of conductive nanocomposites consisting of poly(3-hexylthiophene) (P3HT) and ZnO nanowires in *o*-dichlorobenzene (*o*-DCB) has been investigated rheologically. The physical gelation of P3HT in *o*-DCB spontaneously occurs upon adding the small amount of ZnO nanowires. The rheological properties of the P3HT/ZnO nanocomposite gels have been systematically studied by varying factors such as polymer concentration, nanowire loading, and temperature. The nanocomposite gel exhibits shear-thinning in the low shear rate range and shear-thickening in the high shear rate range. The elastic storage modulus of the nanocomposite gel gradually increases with gelation time and is consistently independent of frequency at all investigated ranges. The isothermal gelation kinetics has been analyzed by monitoring the storage modulus with gelation time, and the data are well fitted with a first-order rate law. The structural analysis data reveal that the polymer forms the crystalline layer coated on ZnO nanowires. A fringed micelle model is proposed to explain the possible gelation mechanism.

**Keywords:** gelation; conductive polymer composites; ZnO nanowires; rheology



**Citation:** Santos, F.A.; Christensen, D.J., II; Cox, R.Y.; Schultz, S.A.; Fernando, R.H.; Zhang, S. Dynamic Gelation of Conductive Polymer Nanocomposites Consisting of Poly(3-hexylthiophene) and ZnO Nanowires. *J. Compos. Sci.* **2021**, *5*, 199. <https://doi.org/10.3390/jcs5080199>

Academic Editor: Francesco Tornabene

Received: 3 July 2021  
Accepted: 20 July 2021  
Published: 30 July 2021

**Publisher's Note:** MDPI stays neutral with regard to jurisdictional claims in published maps and institutional affiliations.



**Copyright:** © 2021 by the authors. Licensee MDPI, Basel, Switzerland. This article is an open access article distributed under the terms and conditions of the Creative Commons Attribution (CC BY) license (<https://creativecommons.org/licenses/by/4.0/>).

## 1. Introduction

Conductive polymer gels (CPGs) have attracted great interest for potential applications in stretchable electronics, biomedical devices, tissue engineering, supercapacitors, and so on, because of their unique combination of excellent electrical conductivity, good mechanical flexibility, and their ability to form interconnected 3D networks [1–5]. One of the most popular approaches to form CPGs is the gelation of conductive polymers in a poor solvent/good solvent mixture [6–9]. In a good solvent, conductive polymers display a coil-like conformation. Upon the addition of a poor solvent, a coil-to-rod transition spontaneously occurs, resulting in the formation of crystalline nanofibrils via  $\pi$ – $\pi$  stacking of the conjugated backbone [10–13]. When the polymer concentration is above a critical value, the sol–gel transition or gelation will occur, yielding a 3D porous network [14]. Early studies have suggested that the nanofibrils aggregate into the ordered domains that serve as the physical cross-linkers for the formation of the 3D network [8]. Later reports have revealed branching of nanofibrils in the gel [15,16]. Experimental studies [17] and theoretical simulations [18] on the morphological evolution during the sol–gel transition have demonstrated that the nanofibrils form the entangled clusters through fractal aggregation, and subsequently, the gelation occurs due to the percolation transition. Interestingly, polymer entanglement greatly facilitates the development of crystalline nanofibrils, which are further interconnected to form the elastic 3D network [18].

The incorporation of foreign nanoparticles into CPGs can effectively improve the mechanical stability and the chemical functionality of CPGs [19–21]. The resulting conductive polymer nanocomposite gels exhibit unusual chemical and physical properties owing to their synergistic effects. It was reported that the composite gels consisting of the conductive

polymer and fullerene were used as a photoactive layer of polymer photovoltaics [22–25]. The gelation increased charge transport and enhanced the interfacial interactions between the polymer donor and fullerene acceptor. As such, the power conversion efficiency of devices fabricated from the composite gel was around six times higher than that of devices from the same solutions without gelation [22]. Recently, the conductive composite gels consisting of polypyrrole and carbon nanotubes were reported by solution mixing of polypyrrole and carbon nanotubes to form interconnected porous networks [26]. The resulting polypyrrole/nanotube nanocomposite gels demonstrated very high conductivity and biocompatibility, and they were further fabricated into the soft biosensors displaying excellent electrochemical sensing of living cells. While the polymer composite gels are promising for the fabrication of high-performance polymer devices, the dynamic process of gelation of conductive polymer nanocomposites is still far from being understood.

In this work, we report on the dynamic sol–gel process of poly(3-hexylthiophene) (P3HT) in the presence of ZnO nanowires in *o*-dichlorobenzene (*o*-DCB). *o*-DCB is a good solvent for P3HT at room temperature, and no gelation occurs in 10 wt % P3HT solution. Interestingly, the addition of 1.0 wt % ZnO nanowires to the same P3HT solution leads to a spontaneous sol–gel transition. With increasing nanowire loading, the critical gelation temperature increases. We have demonstrated gelation kinetics of P3HT/ZnO nanocomposites by investigating the rheological properties. We put forward arguments to explain the spontaneous gelation of P3HT/ZnO nanocomposites.

## 2. Materials and Methods

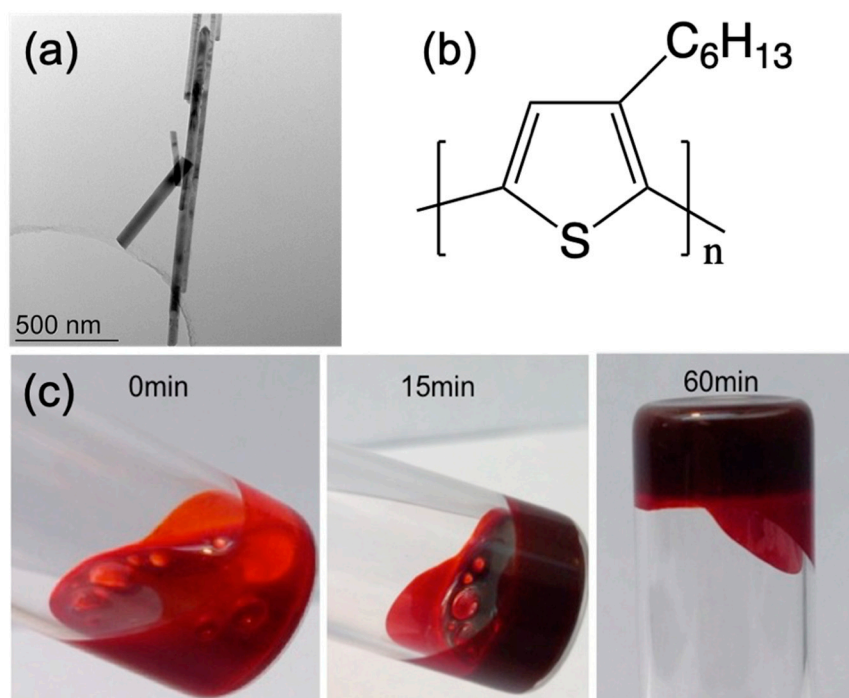
All chemical reagents were used as received without any further purification. Poly(3-hexylthiophene) (P3HT) with regioregularity of 91–94% and average molecular weight of 50–70 kg/mol was purchased from Rieke Metals Inc., Lincoln, NE, USA. Zinc oxide (ZnO) nanowires were prepared using low-temperature solvothermal synthesis [27,28] and modified with 1-dodecanethiol (DDT) to increase miscibility with P3HT [29]. Gel samples were prepared by mixing P3HT and DDT modified ZnO nanowires in *o*-dichlorobenzene (*o*-DCB) using a Branson 2510 bath sonicator at 60 °C for 30 min to get homogeneous solutions. Subsequently, the solution was removed from the sonication bath and allowed to stand at room temperature to obtain complete gelation before any measurements were performed.

Transmission electron microscopic (TEM) images were obtained with a Hitachi HF2000 microscope operated at an acceleration voltage of 110 kV. UV-visible (UV-Vis) absorption spectra of solution samples were obtained at room temperature on a Jasco V-550 spectrophotometer with a cell of quartz cuvette (1.0 cm path length) without stirring. Rheological measurements were performed using TA Instruments Discovery HR-2 rheometer equipped with a 40 mm, 2° cone. A 55 µm gap between the truncated tip of the cone and bottom Peltier plate was maintained. Viscosities were measured under a steady-state flow mode in the shear rate range of 0.01–1000 s<sup>-1</sup>. Dynamic oscillatory measurements were performed with a 1.0% strain and at a frequency of 1.0 Hz unless otherwise noted. For gelation kinetic measurements, gels were heated and liquefied using a bath sonicator at 60 °C. Once liquefied, the solution was rapidly loaded onto the rheometer at the preset temperature for data collection.

## 3. Results and Discussion

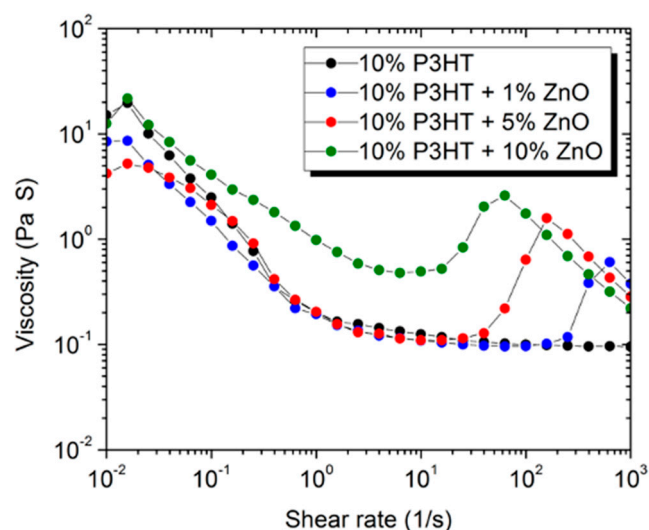
The single crystalline ZnO nanowires were prepared in our laboratory using solvothermal synthesis and were subsequently surface-modified by the direct attachment of an aliphatic ligand, 1-dodecanethiol (DDT), as previously reported [29]. The resulting ZnO nanowires were polydisperse with an average diameter of ≈30 nm, as revealed by TEM (Figure 1a). DDT-modified ZnO nanowires were highly dispersible in organic solvents such as *o*-dichlorobenzene (*o*-DCB). The conductive polymer in this work is the benchmark conductive polymer material, poly(3-hexylthiophene) (P3HT), and its chemical structure is shown in Figure 1b. P3HT was highly soluble in *o*-DCB at room temperature, and

the solution containing 10 wt % P3HT exhibited fluidity without gelation. Interestingly, adding 1.0 wt % ZnO nanowires into the same solution of P3HT led to a spontaneous sol–gel transition at room temperature (Figure 1c). The resulting composite gel exhibited a dark-brownish color. With increasing the loading of nanowires, gelation became instant, and the brownish color of the gel turned darker.



**Figure 1.** (a) TEM image of DDT-modified ZnO nanowires; (b) chemical structure of P3HT; (c) the sol–gel transition of 10 wt % P3HT in *o*-DCB with 1.0 wt % ZnO nanowires at room temperature.

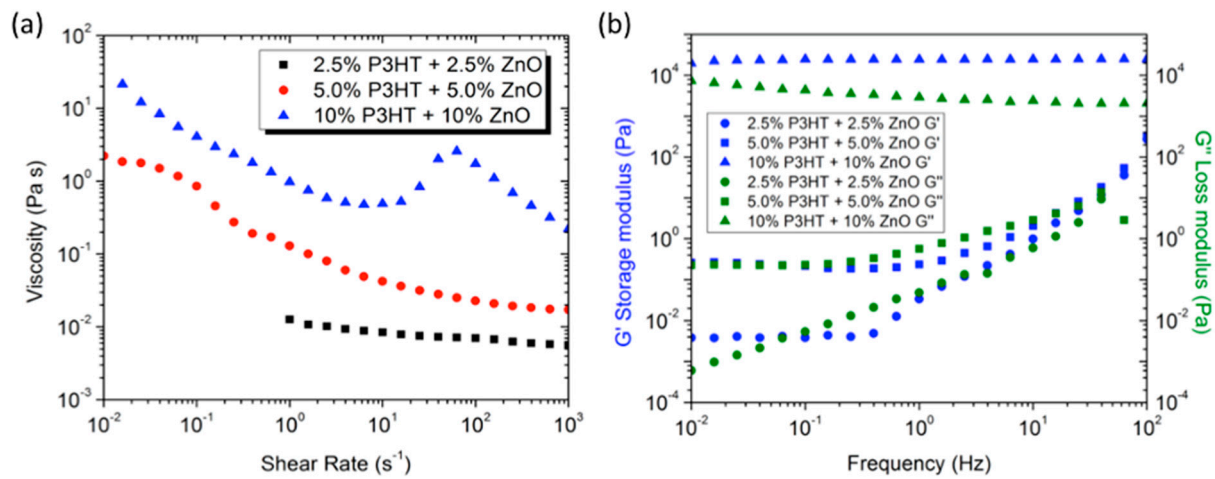
To study the evolution of microstructures during the gelation of P3HT/ZnO nanocomposites, the rheological behavior of the composite gel was investigated. Figure 2 shows the rheological data of the steady shear viscosity versus shear rate of the 10 wt % P3HT solution in *o*-DCB before and after the addition of various amounts of ZnO nanowires. The control P3HT solution exhibits shear-thinning, which is a typical rheological behavior of the concentrated solution of the conductive polymer [30]. This non-Newtonian behavior is attributed to the disruption of weak entanglements of polymer chains under the shear stress [15]. Upon the addition of ZnO nanowires, the P3HT solution displays an initial shear-thinning effect at the low shear rate range, which is followed by a shear-thickening behavior at the high shear rate range. After the shear-thickening peak, the viscosity drops with shear rate. With increasing loading of ZnO nanowires, the onset of shear-thickening shifts toward a low shear rate. The shear-thickening behavior observed in this work is in contrast with that of P3HT gels in a marginal solvent. The latter consistently shows a shearing-thinning behavior in the whole shear rate range [31]. Evidently, ZnO nanowires play a crucial role in the development of shear-thickening of P3HT gels in *o*-DCB. It is believed that the interfacial interactions between P3HT and ZnO nanowires [29] and aggregations of ZnO nanowires under the high shear stress contribute to the shear-thickening behavior in this system. At shear rates above the shear-thickening peak, the breakdown of microstructures of ZnO nanowires leads to a viscosity fall.



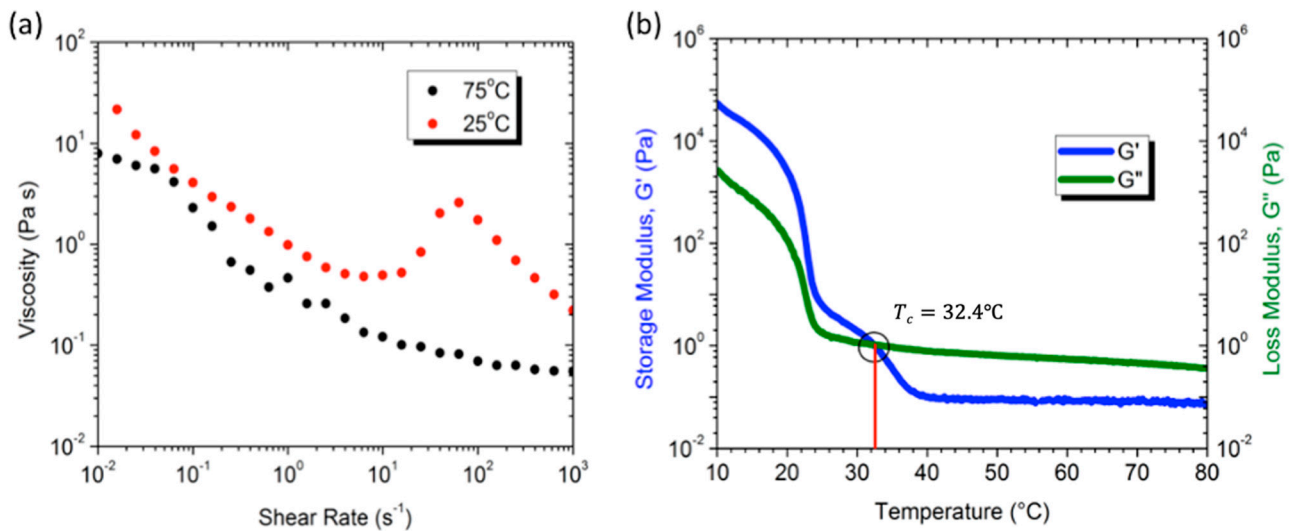
**Figure 2.** Steady shear viscosity versus shear rate data for 10 wt % P3HT in *o*-DCB at room temperature with different loadings of ZnO nanowires.

Figure 3 show the effect of polymer concentration on the gelation and rheology of P3HT/ZnO mixture at the constant 1:1 weight ratio of P3HT:ZnO. In the semi-dilute solutions, 2.5 wt % and 5.0 wt % P3HT with ZnO nanowires at room temperature formed viscous solutions, and no gelation was observed. However, in the concentrated solution of 10 wt % P3HT with 10 wt % ZnO nanowires, the nanocomposite formed a complete gel. Figure 3a displays the steady shear viscosity versus shear rate data of P3HT solutions and gels. As expected, the viscous solutions of 2.5 wt % and 5.0 wt % P3HT with ZnO nanowires display shear-thinning in the whole shear rate range, while the gels of 10 wt % P3HT with 10 wt % ZnO nanowires demonstrate the shear-thickening effect in the high shear rate range. This implies that the shear thickening behavior is strongly correlated with gelation of the concentrated solution of P3HT with ZnO nanowires. To further probe this, the viscoelastic properties of P3HT/ZnO gels were investigated using dynamic oscillatory measurements of the storage modulus  $G'$  and loss modulus  $G''$  data, as shown in Figure 3b. In general, the  $G'$  reveals the elastic properties, whereas the  $G''$  demonstrates the viscous behavior of a material [27]. It is found that the values of both  $G'$  and  $G''$  are comparable in the solutions of 2.5 wt % and 5.0 wt % P3HT with ZnO nanowires, and they tend to increase in the high-frequency range. This phenomenon indicates that the materials are viscoelastic fluids [32]. For the physical gel of 10 wt % P3HT with 10 wt % ZnO nanowires, the material behaves as a viscoelastic solid, where the  $G'$  value is higher than the  $G''$  value and both values are virtually independent of frequency at all investigated ranges. This observation indicates the quasi-solid nature of the gel, which is in good agreement with the literature reports on the polymer gels [33].

In this work, we found that the sol–gel transition of P3HT/ZnO nanocomposites in *o*-DCB was thermally reversible. At high temperatures, the homogeneous mixture was thermodynamically stable. Upon cooling, the mixture became supersaturated with a high degree of super-cooling, and thereafter, gelation occurred. To study the effect of temperature on gelation, the steady shear viscosity was determined at 25 °C and 75 °C, respectively (Figure 4a). At 25 °C, the system formed a physical gel, demonstrating shear-thickening behavior in the high shear rate range. Increasing the temperature disrupts the network of the gel accompanied by a decrease in the viscosity of the material. The system became a viscous mixture at 75 °C, exhibiting only shear thinning. The heating–cooling cycles were repeated, and there was no observable disruption of the sol–gel transition.



**Figure 3.** Rheological data of P3HT/ZnO nanocomposite solutions in *o*-DCB at 1:1 weight ratio of P3HT:ZnO with different polymer concentration at room temperature. (a) Steady shear viscosity versus shear rate and (b) frequency dependence of storage modulus and loss modulus.



**Figure 4.** Effect of temperature on the rheological properties of 10 wt % P3HT/ZnO gels in *o*-DCB with at 1:1 weight ratio of P3HT:ZnO. (a) Steady shear viscosity versus shear rate and (b) temperature dependence of the storage modulus and loss modulus during cooling.

To evaluate the gelation point with respect to temperature, the viscoelastic properties of the system were studied via a temperature sweep from 80 to 10 °C (Figure 4b). At high temperature, the loss modulus  $G''$  is higher than the storage modulus  $G'$ , implying that the material is a viscous fluid. With decreasing the temperature, the values of  $G'$  and  $G''$  increase accordingly. Below the critical temperature  $T_c$ , the  $G'$  becomes dominant over the  $G''$ , and therefore, the material becomes a viscoelastic solid. This observation may be attributed to the threshold of gelation with the development of 3D networks [33]. The sol–gel transition temperature was determined from the intersection point between the  $G'$  and  $G''$ . Figure 4b shows that the critical gelation temperature ( $T_c$ ) of 10 wt % P3HT with 10 wt % ZnO nanowires in *o*-DCB is 32.4 °C. We used this approach to study the effect of ZnO nanowire loading on the critical gelation temperature. Table 1 summarizes the critical gelation temperatures of various P3HT/ZnO nanocomposite gels with different ZnO nanowire loading. It can be seen that increasing ZnO nanowires loading leads to enhancement of gelation temperature, indicating that the addition of ZnO nanowires promotes the thermal stability of the gel.

**Table 1.** Critical gelation temperature ( $T_c$ ) of P3HT/ZnO nanocomposites in *o*-DCB with various ZnO loading.

P3HT/ZnO Gels <sup>(a)</sup>	1.0 wt % ZnO	5.0 wt % ZnO	10 wt % ZnO
$T_c$ ( $^{\circ}\text{C}$ )	21.0	21.8	32.4

<sup>(a)</sup> The concentration of P3HT in *o*-DCB was set to be 10 wt %.

To understand the dynamic process of gelation, the kinetics of the sol–gel transition of 10 wt % P3HT with 10 wt % ZnO nanowires in *o*-DCB at different temperature were investigated using isothermal time dependence of the storage modulus  $G'$  (Figure 5a). When temperature was below the critical gelation temperature  $T_c$ , the storage modulus  $G'$  increased dramatically over the gelation time and leveled off to become time independent at long times. It is found that the magnitude of the elevation in  $G'$  decreases with increasing temperature, and the gelation time when  $G'$  levels off increases with increasing temperature. This observation is attributed to the evolution of the gelation process [34]. The degree of conversion ( $X(t)$ ) is correlated with the change of storage modulus and defined by Equation (1) [35]:

$$X(t) = \frac{G'(t) - G'(0)}{G'(max) - G'(0)} \quad (1)$$

where  $G'(t)$  and  $G'(0)$  represent the storage moduli at gelation time  $t$  and the start of the experiment, respectively;  $G'(max)$  is the storage modulus at the maximum gelation time. Figure 5b shows the plots of the degree of conversion as a function of gelation time at three different temperatures. It can be seen that the conversion degree of gelation is almost zero before the onset of the gelation process followed by a significant increase with gelation time. The maximum degree of conversion is below unity, indicating a slow and incomplete gelation process over the time scale of the observation. It can be seen that decreasing the temperature enhances the conversion degree of gelation.

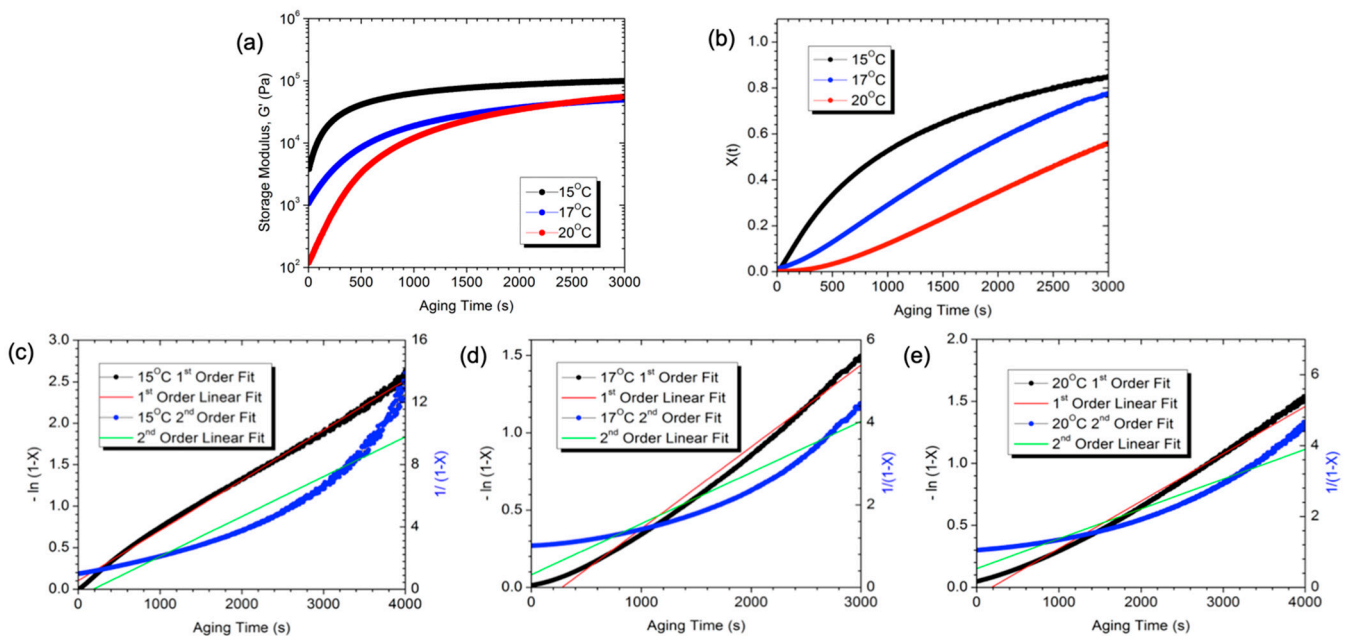


**Figure 5.** Kinetics of the sol–gel process of 10 wt % P3HT/ZnO gels with at 1:1 weight ratio of P3HT:ZnO in *o*-DCB at different temperature. (a) Storage modulus versus aging time; (b) gelation conversion degree versus aging time, and (c–e) plots of gelation conversion degree versus aging time based on first-order and second-order rate laws at different temperature: (c) 15  $^{\circ}\text{C}$ , (d) 17  $^{\circ}\text{C}$ , and (e) 20  $^{\circ}\text{C}$ .

In general, the polymer gelation follows either a first-order [36–38] or a second-order [39–41] kinetic process, depending on the polymer structure, molecular weight, and

crosslinking mechanism. Using the data obtained in this work, two simple integrated rate law equations can be applied by Equations (2) and (3) [35]:

$$-\ln[1 - X(t)] = k_1 t \quad (2)$$

$$\frac{1}{[1 - X(t)]} = k_2 t + 1 \quad (3)$$

where Equations (2) and (3) represent first-order and second-order gelation kinetics, respectively. Figure 5c–e show the best-fit straight lines of the data at three different temperatures using Equations (2) and (3). It is evident that the gelation of P3HT/ZnO nanocomposites in *o*-DCB is better described by a first-order rate law compared to a second-order rate law. This observation is in accordance with the literature reports of crystallization-induced polymer gelation [36–38].

UV-vis spectroscopic analysis was used to understand the physical origin of the gelation process. Figure 6a displays UV-Vis absorption spectra of the solution samples diluted from 10 wt % P3HT/ZnO nanocomposite gels with different amounts of ZnO nanowires in *o*-DCB. The sample diluted from the control P3HT in *o*-DCB displayed an absorption maximum at  $\lambda \approx 460$  nm, indicating the random coil-like conformation of P3HT chains in *o*-DCB [10]. This phenomenon is well known as the P3HT molecules completely dissolve in *o*-DCB due to their similar solubility parameters of  $\delta_{P3HT} = 19.27 \text{ J}^{1/2}/\text{cm}^{3/2}$  and  $\delta_{o\text{-DCB}} = 19.58 \text{ J}^{1/2}/\text{cm}^{3/2}$  [14]. The diluted composite gels showed little change in the wavelength ( $\lambda \approx 460$  nm) of the absorption maximum, but a new weak absorption peak emerged at  $\lambda \approx 600$  nm. By increasing the amount of ZnO nanowires in the composite gel, the absorption intensity of the new low energy band at  $\lambda \approx 600$  nm also increased. In general, this new low energy vibronic band is associated with the rod-like conformation of polymer chains and electronic interactions of the polymer backbones in the crystalline state owing to the interactional interactions between the conductive polymer and foreign nanoparticles [29,42,43]. Therefore, P3HT chains on ZnO nanowire surfaces undergo a coil-to-rod transition to form crystals [29]. This was further confirmed by high-resolution TEM that showed ZnO nanowires coated with a crystalline layer of P3HT (Figure 6b). This observation is expected because ZnO nanowires serve as an orientation template and heterogeneous nucleation agent for conjugated polymer crystallization. A recent study has illustrated a significant decrease in the energy barrier of P3HT crystallization upon adding DDT-modified ZnO nanowires owing to their favorable van der Waals interfacial interactions [29].

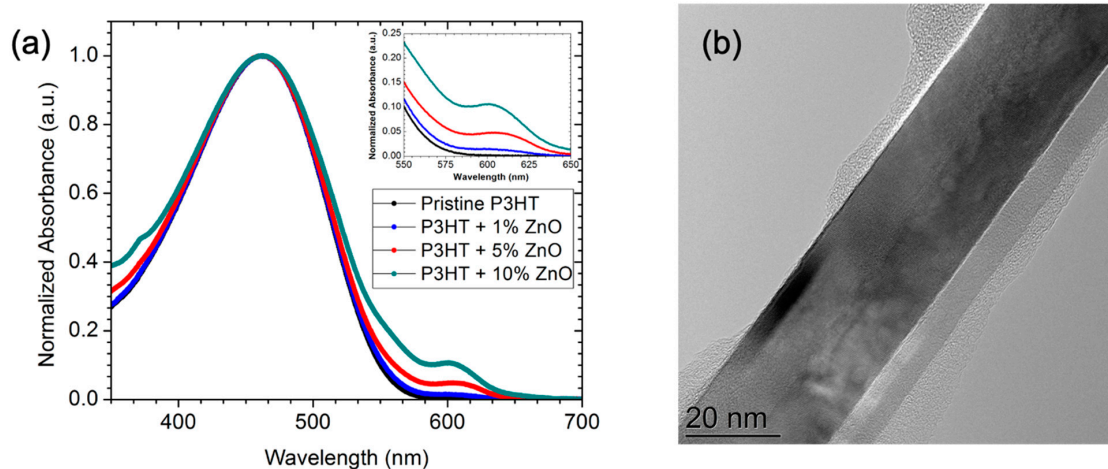


**Figure 6.** (a) UV-vis absorption spectra of solution samples diluted from 10 wt % P3HT gels with different amounts of ZnO nanowires in *o*-DCB and (b) TEM image of the diluted P3HT/ZnO gel revealing a P3HT crystal layer coated on the ZnO nanowire surface.

The sol–gel transition of P3HT/ZnO nanowires in *o*-DCB presented in this work is different from that of P3HT in a marginal solvent. First, the shear-thickening behavior is unique in P3HT/ZnO nanocomposite gels. Second, the gelation of P3HT/ZnO nanocomposites only occurs in the concentrated solution. Third, the P3HT/ZnO nanocomposite gel is dominated by the coil-like chain structures with small amounts of crystals. Based on these observations, a possible gelation mechanism is proposed, as shown in Figure 7. The pure P3HT in *o*-DCB forms an amorphous phase with the coil-like conformation, and therefore, no gelation occurs. In the P3HT/ZnO nanocomposite mixture, ZnO nanowires serve as an orientational template and heterogeneous nucleation agent for P3HT crystallization [29]. The resulting ordered P3HT crystals on the surfaces of ZnO nanowires are bundle-like with amorphous coil-like chains emanating from the bundles. The ordered crystals attached on ZnO nanowires serve as physical cross-linkers to connect the coil-like chains to form interconnected networks. This gelation mechanism is analogous to the well-known fringed micelle model of crystallization-induced polymer gelation [36–38]. Under the strong shear stress, the P3HT crystal-coated ZnO nanowires tend to aggregate in the matrix of coil-like polymer chains, yielding a shear-thickening effect (Figure 7). As the coil-like polymer chains are predominant in the gel, the polymer concentration must be high enough to maintain the connectedness necessary for gelation.

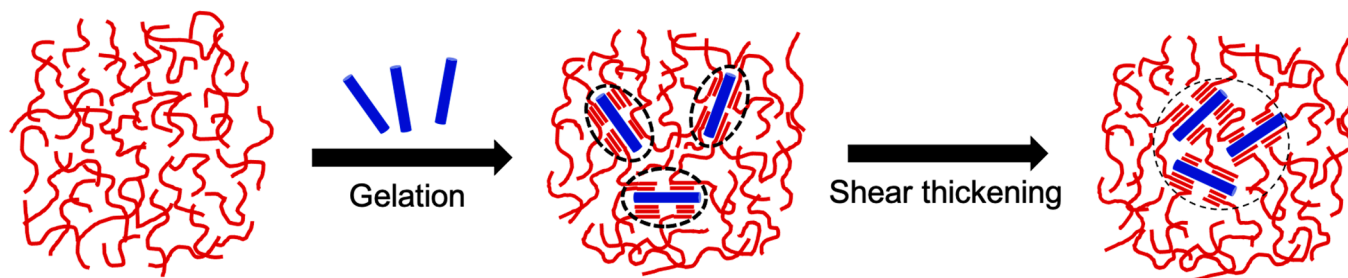


**Figure 7.** Schematic representation of physical cross-linking mechanism of P3HT by the addition of ZnO nanowires in *o*-DCB and shear thickening mechanism. Dashed cycles highlight the cross-linkers consisting of nanowires and polymer crystals.

#### 4. Conclusions

In summary, we have reported on the sol–gel process of poly(3-hexylthiophene) (P3HT)/ZnO nanocomposites in *o*-dichlorobenzene (DCB) using rheological methods. P3HT forms a crystal layer coated on ZnO nanowires owing to the strong interfacial interactions. P3HT crystal-coated ZnO nanowires act as physical cross-linkers to connect the adjacent coil-like P3HT chains, generating a solid-like gel. Under strong shear stress, ZnO nanowires aggregate together, leading to a shear-thickening phenomenon. Increasing the ZnO nanowire loading or decreasing the temperature promotes the occurrence of physical gelation. The gelation conversion as a function of gelation time reveals a first-order rate law in the sol–gel process of P3HT/ZnO nanocomposites. As a result of recent advances in gel printing of high-performance devices, our work may be of importance in exploring conductive polymer nanocomposite gels for next-generation devices.

**Author Contributions:** Conceptualization: S.Z.; Methodology: S.Z.; formal analysis: F.A.S. and S.Z.; investigation: F.A.S., D.J.C.II, R.Y.C. and S.A.S.; resources: R.H.F.; writing—original draft preparation: F.A.S. and S.Z.; writing-review and editing: S.Z. and R.H.F.; supervision: S.Z.; funding acquisition: S.Z. All authors have read and agreed to the published version of the manuscript.

**Funding:** This research was funded by the National Science Foundation (CMMI-1345138) and Cal Poly Extramural Funding Initiative.

**Acknowledgments:** S.Z. acknowledges the financial support from American Chemistry Society-Petroleum Research Fund (53970-UR7). F.A.S. acknowledges the financial support from Cal Poly Bill Moore Fellowship.

**Conflicts of Interest:** The authors declare no conflict of interest.

## References

1. Zhao, Y.; Liu, B.; Pan, L.; Yu, G. 3D nanostructured conductive polymer hydrogels for high-performance electrochemical devices. *Energy Environ. Sci.* **2013**, *6*, 2856–2870. [[CrossRef](#)]
2. Zhang, W.; Feng, P.; Chen, J.; Sun, Z.; Zhao, B. Electrically conductive hydrogels for flexible energy storage systems. *Prog. Polym. Sci.* **2019**, *88*, 220–240. [[CrossRef](#)]
3. Shi, H.; Dai, Z.; Sheng, X.; Xia, D.; Shao, P.; Yang, L.; Luo, X. Conducting polymer hydrogels as a sustainable platform for advanced energy, biomedical and environmental applications. *Sci. Total Environ.* **2021**, *786*, 147430. [[CrossRef](#)]
4. Zhao, F.; Shi, Y.; Pan, L.; Yu, G. Multifunctional Nanostructured Conductive Polymer Gels: Synthesis, Properties, and Applications. *Acc. Chem. Res.* **2017**, *50*, 1734–1743. [[CrossRef](#)]
5. Nezakati, T.; Seifalian, A.; Tan, A.; Seifalian, A.M. Conductive Polymers: Opportunities and Challenges in Biomedical Applications. *Chem. Rev.* **2018**, *118*, 6766–6843. [[CrossRef](#)] [[PubMed](#)]
6. Li, S.; He, K.; Prince, E.; Li, Y.; Seferos, D.S. Selenophene and Thiophene-Based Conjugated Polymer Gels. *ACS Mater. Lett.* **2020**, *2*, 1617–1623. [[CrossRef](#)]
7. Bilger, D.W.; Figueroa, J.A.; Redeker, N.D.; Sarkar, A.; Stefk, M.; Zhang, S. Hydrogen-Bonding-Directed Ordered Assembly of Carboxylated Poly(3-Alkylthiophene)s. *ACS Omega* **2017**, *2*, 8526–8535. [[CrossRef](#)]
8. Malik, S.; Jana, T.; Nandi, A.K. Thermoreversible gelation of regioregular poly(3-hexylthiophene) in xylene. *Macromolecules* **2001**, *34*, 275–282. [[CrossRef](#)]
9. Chang, M.Y.; Huang, Y.H.; Han, Y.K. Aggregation, crystallization, and resistance properties of poly(3-hexylthiophene-2,5-diyl) solid films gel-cast from CHCl<sub>3</sub>/p-xylene mixed solvents. *Org. Electron.* **2014**, *15*, 251–259. [[CrossRef](#)]
10. Bilger, D.; Sarkar, A.; Danesh, C.; Gopinadhan, M.; Braggin, G.; Figueroa, J.; Pham, T.V.; Chun, D.; Rao, Y.; Osuji, C.O.; et al. Multi-Scale Assembly of Polythiophene-Surfactant Supramolecular Complexes for Charge Transport Anisotropy. *Macromolecules* **2017**, *50*, 1047–1055. [[CrossRef](#)]
11. Danesh, C.D.; Starkweather, N.S.; Zhang, S. In situ study of dynamic conformational transitions of a water-soluble poly(3-hexylthiophene) derivative by surfactant complexation. *J. Phys. Chem. B* **2012**, *116*, 12887–12894. [[CrossRef](#)]
12. Zhang, S.; Pfefferle, L.D.; Osuji, C.O. Lyotropic hexagonal ordering in aqueous media by conjugated hairy-rod supramolecules. *Macromolecules* **2010**, *43*, 7549–7555. [[CrossRef](#)]
13. Brinkmann, M. Structure and morphology control in thin films of regioregular poly(3-hexylthiophene). *J. Polym. Sci. Part B Polym. Phys.* **2011**, *49*, 1218–1233. [[CrossRef](#)]
14. Chen, C.Y.; Chan, S.H.; Li, J.Y.; Wu, K.H.; Chen, H.L.; Chen, J.H.; Huang, W.Y.; Chen, S.A. Formation and thermally-induced disruption of nanowhiskers in poly(3-hexylthiophene)/Xylene gel studied by small-angle X-ray scattering. *Macromolecules* **2010**, *43*, 7305–7311. [[CrossRef](#)]
15. Newbloom, G.M.; Weigandt, K.M.; Pozzo, D.C. Structure and property development of poly(3-hexylthiophene) organogels probed with combined rheology, conductivity and small angle neutron scattering. *Soft Matter* **2012**, *8*, 8854–8864. [[CrossRef](#)]
16. Newbloom, G.M.; Kim, F.S.; Jenekhe, S.A.; Pozzo, D.C. Mesoscale morphology and charge transport in colloidal networks of poly(3-hexylthiophene). *Macromolecules* **2011**, *44*, 3801–3809. [[CrossRef](#)]
17. Newbloom, G.M.; De La Iglesia, P.; Pozzo, L.D. Controlled gelation of poly(3-alkylthiophene)s in bulk and in thin-films using low volatility solvent/poor-solvent mixtures. *Soft Matter* **2014**, *10*, 8945. [[CrossRef](#)] [[PubMed](#)]
18. Lee, C.K.; Hua, C.C.; Chen, S.A. Phase transition and gels in conjugated polymer solutions. *Macromolecules* **2013**, *46*, 1932–1938. [[CrossRef](#)]
19. Ma, Z.; Shi, W.; Yan, K.; Pan, L.; Yu, G. Doping engineering of conductive polymer hydrogels and their application in advanced sensor technologies. *Chem. Sci.* **2019**, *10*, 6232–6244. [[CrossRef](#)] [[PubMed](#)]
20. Liu, Z.; Zhao, Z.; Xu, A.; Li, W.; Qin, Y. Facile preparation of graphene/polyaniline composite hydrogel film by electrodeposition for binder-free all-solid-state supercapacitor. *J. Alloys Compd.* **2021**, *875*, 159931. [[CrossRef](#)]
21. Zhai, D.; Liu, B.; Shi, Y.; Pan, L.; Wang, Y.; Li, W.; Zhang, R.; Yu, G. Highly Sensitive Glucose Sensor Based on Pt Nanoparticle/Polyaniline Hydrogel Heterostructures. *ACS Nano* **2013**, *7*, 3540–3546. [[CrossRef](#)]
22. Li, P.; Chen, L.J.; Pan, J.; Niu, G.X.; Zhang, T.; Xiang, J.; Cai, L.; Hu, Y.; Zhang, Y.J.; Wan, K.M.; et al. Dispersion of P3HT gelation and its influence on the performance of bulk heterojunction organic solar cells based on P3HT:PCBM. *Sol. Energy Mater. Sol. Cells* **2014**, *125*, 96–101. [[CrossRef](#)]
23. Kim, B.G.; Jeong, E.J.; Park, H.J.; Bilby, D.; Guo, L.J.; Kim, J. Effect of polymer aggregation on the open circuit voltage in organic photovoltaic cells: Aggregation-induced conjugated polymer gel and its application for preventing open circuit voltage drop. *ACS Appl. Mater. Interfaces* **2011**, *3*, 674–680. [[CrossRef](#)] [[PubMed](#)]
24. Zuo, L.J.; Hu, X.L.; Ye, T.; Andersen, T.R.; Li, H.Y.; Shi, M.M.; Xu, M.; Ling, J.; Zheng, Q.; Xu, J.T.; et al. Effect of solvent-assisted nanoscaled organo-gels on morphology and performance of organic solar cells. *J. Phys. Chem. C* **2012**, *116*, 16893–16900. [[CrossRef](#)]
25. Huang, W.Y.; Huang, P.T.; Han, Y.K.; Lee, C.C.; Hsieh, T.L.; Chang, M.Y. Aggregation and gelation effects on the performance of poly(3-hexylthiophene)/fullerene solar cells. *Macromolecules* **2008**, *41*, 7485–7489. [[CrossRef](#)]
26. Yang, M.; Ren, X.; Yang, T.; Xu, C.; Ye, Y.; Sun, Z.; Kong, L.; Wang, B.; Luo, Z. Polypyrrole/sulfonated multi-walled carbon nanotubes conductive hydrogel for electrochemical sensing of living cells. *Chem. Eng. J.* **2021**, *418*, 129483. [[CrossRef](#)]

27. Cox, R.; Olson, G.T.; Pfau, M.; Eshaghi, N.; Barcus, K.; Ramirez, D.; Fernando, R.; Zhang, S. Solution-Based Large-Area Assembly of Coaxial Inorganic—Organic Hybrid Nanowires for Fast Ambipolar Charge Transport. *ACS Appl. Mater. Interfaces* **2017**, *9*, 3–9. [[CrossRef](#)]
28. Redeker, N.D.; Danesh, C.D.; Ding, Y.; Zhang, S. Anisotropic core-shell nanocomposites by direct covalent attachment of a side-functionalized poly(3-hexylthiophene) onto ZnO nanowires. *Polymer* **2013**, *54*, 7004–7008. [[CrossRef](#)]
29. Wagner, T.W.; Luo, Y.; Redeker, N.D.; Immoos, C.E.; Zhang, S. Effect of surface-modified zinc oxide nanowires on solution crystallization kinetics of poly(3-hexylthiophene). *Polymer* **2014**, *55*, 2008–2013. [[CrossRef](#)]
30. Koppe, M.; Brabec, C.J.; Heiml, S.; Schausberger, A.; Duffy, W.; Heeney, M.; McCulloch, I. Influence of molecular weight distribution on the gelation of P3HT and its impact on the photovoltaic performance. *Macromolecules* **2009**, *42*, 4661–4666. [[CrossRef](#)]
31. Xu, W.; Tang, H.; Lv, H.; Li, J.; Zhao, X.; Li, H.; Wang, N.; Yang, X. Sol-gel transition of poly(3-hexylthiophene) revealed by capillary measurements: Phase behaviors, gelation kinetics and the formation mechanism. *Soft Matter* **2012**, *8*, 726–733. [[CrossRef](#)]
32. Shafiei-Sabet, S.; Hamad, W.Y.; Hatzikiriakos, S.G. Rheology of nanocrystalline cellulose aqueous suspensions. *Langmuir* **2012**, *28*, 17124–17133. [[CrossRef](#)] [[PubMed](#)]
33. Yi, H.L.; Hua, C.C. PBTTC-C16 sol-gel transition by rod associations and networking. *Soft Matter* **2019**, *15*, 8022–8031. [[CrossRef](#)] [[PubMed](#)]
34. Madbouly, S.A.; Otaigbe, J.U. Kinetic analysis of fractal gel formation in waterborne polyurethane dispersions undergoing high deformation flows. *Macromolecules* **2006**, *39*, 4144–4151. [[CrossRef](#)]
35. Xie, F.; Weiss, P.; Chauvet, O.; Le Bideau, J.; Tassin, J.F. Kinetic studies of a composite carbon nanotube-hydrogel for tissue engineering by rheological methods. *J. Mater. Sci. Mater. Med.* **2010**, *21*, 1163–1168. [[CrossRef](#)]
36. Dudukovic, N.A.; Zukoski, C.F. Gelation of Fmoc-diphenylalanine is a first order phase transition. *Soft Matter* **2015**, *11*, 7663–7673. [[CrossRef](#)]
37. Auriemma, F.; De Rosa, C.; Triolo, R. Slow crystallization kinetics of poly(vinyl alcohol) in confined environment during cryotropic gelation of aqueous solutions. *Macromolecules* **2006**, *39*, 9429–9434. [[CrossRef](#)]
38. Girolamo, M.; Keller, A.; Miyasaka, K.; Overbergh, N. Gelatin-Crystallization in Isotactic Polystyrene Solutions and Its Implications To Crystal Morphology, To the Origin and Structure of Gels, and To the Chemical Homogeneity of Polyolefins. *J. Polym. Sci.* **1976**, *14*, 39–61. [[CrossRef](#)]
39. Normand, V.; Muller, S.; Ravey, J.C.; Parker, A. Gelation kinetics of gelatin: A master curve and network modeling. *Macromolecules* **2000**, *33*, 1063–1071. [[CrossRef](#)]
40. Ross-Murphy, S.B. Gelation kinetics—Problems and prospects. *J. Macromol. Sci. Part B Phys.* **2005**, *44*, 1007–1019. [[CrossRef](#)]
41. Shibayama, M. Exploration of ideal polymer networks. *Macromol. Symp.* **2017**, *372*, 7–13. [[CrossRef](#)]
42. Luo, Y.; Santos, F.A.; Wagner, T.W.; Tsoi, E.; Zhang, S. Dynamic Interactions between Poly(3-hexylthiophene) and Single-Walled Carbon Nanotubes in Marginal Solvent. *J. Phys. Chem. B* **2014**, *118*, 6038–6046. [[CrossRef](#)] [[PubMed](#)]
43. Zhang, S.; Bunz, U.H.F.; Bucknall, D.G. Chromatic Conductive Polymer Nanocomposites of Poly(p-Phenylene Ethynylene)s and Single-Walled Carbon Nanotubes. *J. Compos. Sci.* **2021**, *5*, 158. [[CrossRef](#)]